AIAA JOURNAL
Vol. 57, No. 10, October 2019

Composite Blade Twist Modification by Using a Moving Mass and Stiffness Tailoring

M. R. Amoozgar,* A. D. Shaw,† J. Zhang,* and M. I. Friswell‡
Swansea University, Swansea, Wales SA2 8PP, United Kingdom

DOI: 10.2514/1.J057591

In this paper, a new concept for morphing composite blades is proposed, and how this concept changes the twist distribution of the blade is explained. A change in the blade twist is obtained by adding a mass to the blade that produces an extra centrifugal force. This centrifugal force then may produce a moment that can change the blade twist via the extension–twist or bend–twist coupling of the composite lamination. These types of couplings are present in antisymmetrically and symmetrically laminated beams, respectively. The dynamics of the rotating composite blade is modeled by using the geometrically exact fully intrinsic beam equations. The concentrated mass is considered as a nonstructural concentrated mass that has offsets with respect to the beam reference line. The nonlinear partial differential equations are discretized by using a time–space scheme, the converged results are compared with those reported in the literature, and very good agreement is observed. It is found that, for an antisymmetric lamination, the spanwise location of the concentrated mass affects the twist, whereas in the symmetric case, the chordwise position of the concentrated mass is the source of twist change. It is also found that introducing the concentrated mass to a real blade can change the twist dramatically.

Nomenclature

A, B, D	=	stiffness matrices of the cross section
c	=	blade chord
$\boldsymbol{F}, \boldsymbol{M}$	=	internal force and moment
$\boldsymbol{H}, \boldsymbol{P}$	=	linear and angular momenta
$\boldsymbol{k}, \boldsymbol{K}$	=	initial and final curvature vectors
L	=	blade length
q	=	twist angle
$\boldsymbol{V}, \boldsymbol{\Omega}$	=	linear and angular velocities
x_p, y_p, z_p	=	concentrated mass location along x, y, and z coordinates
$\boldsymbol{\gamma}, \boldsymbol{\kappa}$	=	generalized strains
α	=	nondimensional bend–twist coupling term
β	=	concentrated mass ratio
θ	=	ply angle
Ω_0	=	rotor speed

I. Introduction

ROTORCRAFT have many operational advantages over fixed-wing aircraft for missions such as search and rescue and transport to inaccessible terrain [1]. Today's rotorcraft need to improve to be more environmentally friendly in terms of low levels of noise, pollution, fuel consumption, and high levels of performance and comfort, etc. To achieve this aim, morphing rotor blades are a candidate solution, and some new concepts have been proposed. These concepts all promise to enhance the performance or to reduce the noise and vibration of the rotorcraft by changing the shape of the blade, which then modifies the aerodynamic domain. Morphing technology has received widespread attention for fixed-wing aircraft [2], but relatively less literature considers morphing concepts applied to rotorcraft. Among all possible concepts for morphing a blade, the twist and trailing-edge flap concepts have received the most attention over the past two decades [3]. Several different ideas for the control of a blade (including twist, pitch, flap, and camber) have been reviewed by Straub [4] and Chopra [5], and the advantages and disadvantages of these methods for vibration reduction have been reported. The change in the blade twist during flight is the focus of this paper. When a rotorcraft is in the hover condition, highly twisted blades are optimal, whereas low levels of twist are optimal for high-speed forward velocities [6]. Therefore, the predefined blade twist variation normally is chosen as a compromise between different flight conditions. Blade twist morphing changes the blade twist actively during flight to allow the rotorcraft to fly in an optimum condition in terms of twist variation. Han et al. [7] showed how the performance of a helicopter during flight could be improved by dynamic blade twist. They demonstrated that the dynamic blade twist improved the performance and reduced the rotor power requirement.

One of the earliest studies concerning the twist change of the blade via piezoelectric actuators was performed by Chen and Chopra [8]. In their study, the piezoelectric patches were located on the lower and upper surfaces of the blade, and about 0.4 deg of twist change was achieved at 4 rev^{-1}. This concept was tested in hover, and it was found that a linear twist of change of about 0.6 deg might result in a 10% increase in the rotor lift [9]. Chattopadhyay et al. [10] used smart materials to reduce and control the vibratory load of a composite box beam blade. They showed that the number of actuators and their location significantly affected the blade dynamic load reduction. The dynamic behavior of active twist rotor blades with distributed anisotropic strain actuators for vibration and noise reduction purposes has been investigated experimentally and analytically by Cesnik et al. [11]. Good correlation between their developed analytical model and the experimental results has been reported. This study was continued to check the developed analytical model for the forward flight condition by Shin and Cesnik [12]. Thakkar and Ganguli [13] considered the vibration reduction of a soft in-plane hingeless rotor blade in forward flight with induced shear based on piezoceramic actuation. They showed that about a 43% reduction in the vibration was feasible. Schultz [14] proposed a new concept capable of large shape morphing with a small energy input based on bistable structures. The active vibration reduction of composite hingeless rotor blades with dissimilarity based on the active twist concept has been investigated by Pawar and Jung [15]. The numerical results showed that the blade dissimilarities influenced the rotor vibratory loads and the input energy. You et al. [16] examined the influence of different actuation scenarios for

Received 5 June 2018; revision received 1 October 2018; accepted for publication 6 November 2018; published online 31 December 2018.

*Postdoctoral Research Assistant, College of Engineering.
†Lecturer, College of Engineering.
‡Professor, College of Engineering.

maximizing the performance of a rotor in the high-speed flight conditions.

Apart from using piezomaterials for blade morphing, there are some other efforts focusing on using shape memory alloys for blade twist change. Prahlad and Chopra [17] presented the concept of using a shape memory alloy (SMA) torque tube to change the twist distribution of a tiltrotor blade between hover and forward flight. The effect of heat treatment of the SMAs in tuning the actuation behavior was discussed. The development and experiment of an active twist rotor blade using a thermo-mechanical shape memory alloy has been reported by Bushnell et al. [18]. In the Office of Naval Research-funded Reconfigurable Rotor Blade Program, the SMA actuator has been used to change the twist of a V-22 Osprey blade [19–21]. It was shown that about 2 deg of twist change was feasible with this SMA concept [20]. There are also other concepts in the literature for changing the twist of the blades. One concept for twist variation of the blade is the warp-induced twist, which originally was proposed for fixed-wing applications [22] and then extended to rotary wings [6]. In this concept, the ribs can rotate freely around the spar, and the skin is also free to move on the ribs. The warping is generated by creating a relative motion in the spanwise direction by using a threaded rod; when this rod rotates, the result is a twist change of the blade. The aerodynamic and performance improvement of the tiltrotor aircraft by changing the twist distribution of the blade through the extension–twist coupling of the composite lamination was studied by Nixon [23]. It was shown that, by changing the blade twist via extension–twist coupling, the tiltrotor aerodynamic performance could be improved but the stability characteristics of the blade might also be altered. Soykasap and Hodges [24] presented the performance improvement of a tiltrotor aircraft by using an optimization technique. In this paper, the extension–twist coupling and the aeroelastic stability of the composite blade was optimized so that the performance of the aircraft increased. Positioning an absorber in the spanwise [25–27] or chordwise [28,29] locations of a helicopter blade to produce a lag damper has been studied since the late 1990s. It was shown that the embedded chordwise or spanwise absorbers significantly influenced the dynamics and the aeroelastic behavior of the blade. Although these studies were concerned with the effect of mass location on the dynamics of the blade, none of them dealt with the effect of mass movement on the twist change of the composite blade.

In addition to all the morphing concepts mentioned previously, in this paper, a new concept for morphing the twist of a composite blade is introduced and examined. In this concept, the change of the blade twist is obtained by adding a movable mass near the tip of the blade to create a local centrifugal force that then, through the in-plane bend–twist coupling of the composite layup, results in a torsional moment. This torsional moment is then able to change the twist angle of the blade cross section. A potential advantage of this approach is that, although a distributed morphing actuation is achieved across the entire blade, the majority of the blade deforms passively, with the only active element being the actuator for the inertial mass. Therefore, by minimizing the complexity of mechanisms and added to the high-gravity environment of the rotor blade, a highly reliable and robust solution with a relatively low mass penalty can be achieved. This concept is referred to here as twisting with inertia and stiffness tailoring, or TWIST. Although the primary focus of this paper is to find the effective parameters on the twist change of the blade, it should be noted that, by adding the mass to the blade, the dynamics and stability characteristics of the blade change; and this should be considered in the full system optimization.

In this paper, the proposed concept is first introduced and the important parameters are summarized. Then, an analytical model capable of examining this concept on a composite blade is developed and validated. The effect of different system parameters and their influence on the twist of the blade are then studied on a laboratory-scale beam sourced from the literature. Then, through the use of a nondimensional bend–twist coupling parameter, the potential for actuation of a full-scale BO-105 rotor is shown.

II. Description of the Twist Blade Mechanism

Here, a new method for morphing a composite blade is proposed by means of a moving mass. This is done by moving an inertial mass in the chordwise or spanwise direction of a tailored composite blade. The blade has a rectangular close section spar, and the system is shown in Fig. 1.

This movable mass adds an extra centrifugal force to the system. In the first concept, when the mass moves along the span of the blade, a variable centrifugal force induces in the system, which can change the twist of the blade through the extension–twist coupling of the composite layup. On the other hand, in the second concept, it is considered that the mass moves along the chord of the blade; due to the offset between the mass and the shear centre of the section, it produces a variable bending moment. This bending moment can change the twist of the blade through the bend–twist coupling of the composite spar. Therefore, the concentrated mass location and magnitude are two important factors on the blade twist variation in these morphing concepts. In what follows, these two morphing concepts are examined in a scaled composite blade.

III. Formulation

The composite blade is modeled as an elastic beam cantilevered to the rotor hub, and the concentrated mass is simulated as a concentrated mass locating at a predefined position. Here, the concentrated mass locations along different coordinates are denoted by x_p, y_p, and z_p. The motion in the thickness direction of the mass is not considered here. The one-dimensional (1-D) beam behavior is simulated by using the geometrically exact fully intrinsic beam equations [30], which have been used successfully for modeling the beamlike structures [31–33]. Thus,

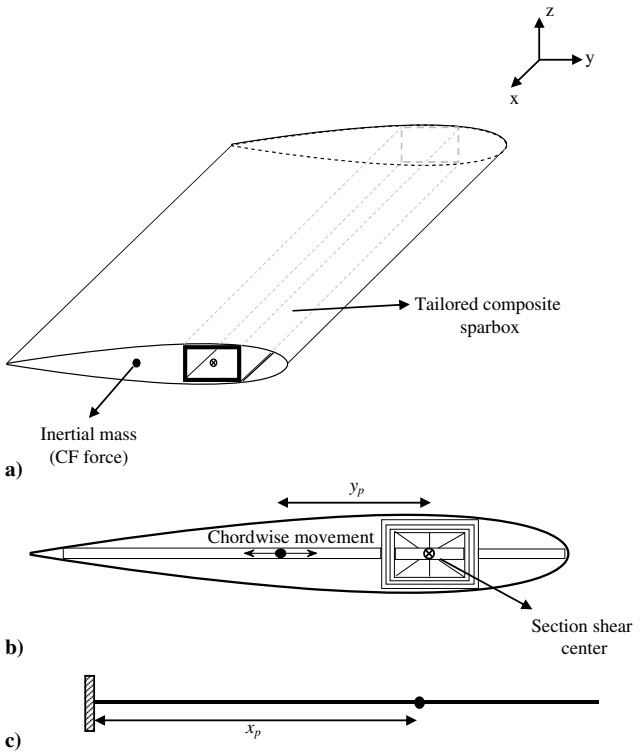

Fig. 1 Schematics of a) the TWIST concept, b) chordwise movement of the mass, and c) spanwise movement of the mass (CF, centrifugal force).

$$
\begin{aligned}
&\partial F_1/\partial x_1 + K_2F_3 - K_3F_2 = \partial P_1/\partial t + \Omega_2P_3 - \Omega_3P_2\\
&\partial F_2/\partial x_1 + K_3F_1 - K_1F_3 = \partial P_2/\partial t + \Omega_3P_1 - \Omega_1P_3\\
&\partial F_3/\partial x_1 + K_1F_2 - K_3F_1 = \partial P_3/\partial t + \Omega_1P_2 - \Omega_2P_1\\
&\partial M_1/\partial x_1 + K_2M_3 - K_3M_2 + 2\gamma_{12}F_3 - 2\gamma_{13}F_2\\
&\quad = \partial H_1/\partial t + \Omega_2H_3 - \Omega_3H_2 + V_2P_3 - V_3P_2\\
&\partial M_2/\partial x_1 + K_3M_1 - K_1M_3 + 2\gamma_{13}F_1 - (1+\gamma_{11})F_3\\
&\quad = \partial H_2/\partial t + \Omega_3H_1 - \Omega_1H_3 + V_3P_1 - V_1P_3\\
&\partial M_3/\partial x_1 + K_1M_2 - K_2M_1 + (1+\gamma_{11})F_2 - 2\gamma_{12}F_1\\
&\quad = \partial H_3/\partial t + \Omega_1H_2 - \Omega_2H_1 + V_1P_2 - V_2P_1\\
&\partial V_1/\partial x_1 + K_2V_3 - K_3V_2 + 2\gamma_{12}\Omega_3 - 2\gamma_{13}\Omega_2 = \partial\gamma_{11}/\partial t\\
&\partial V_2/\partial x_1 + K_3V_1 - K_1V_3 - (1+\gamma_{11})\Omega_3 + 2\gamma_{13}\Omega_1 = 2\partial\gamma_{12}/\partial t\\
&\partial V_3/\partial x_1 + K_1V_2 - K_2V_1 + (1+\gamma_{11})\Omega_2 - 2\gamma_{12}\Omega_1 = 2\partial\gamma_{13}/\partial t\\
&\partial\Omega_1/\partial x_1 + K_2\Omega_3 - K_3\Omega_2 = \partial\kappa_1/\partial t\\
&\partial\Omega_2/\partial x_1 + K_3\Omega_1 - K_1\Omega_3 = \partial\kappa_2/\partial t\\
&\partial\Omega_3/\partial x_1 + K_1\Omega_2 - K_2\Omega_1 = \partial\kappa_3/\partial t
\end{aligned}
\tag{1}
$$

where F_i and M_i for $i = 1, \ldots, 3$ are the internal forces and moments; V_i and Ω_i are the linear and angular velocities; and P_i and H_i are the sectional linear and angular momenta, respectively. The generalized strains of the blade are denoted by γ_{1i} and κ_i, and K_i is the final curvature of the deformed beam that is related to the beam curvature through the following relation:

$$K_i = \kappa_i + k_i \tag{2}$$

where k_i for $i = 1, \ldots, 3$ is the initial curvature and twist of the beam.

All of the quantities mentioned previously are measured in the deformed beam, except for the initial curvature/twist. In this study, it is assumed that the blade does not have any initial twist or curvature. The internal forces and moments are related to the generalized strains by using the stiffness matrix as follows:

$$
\begin{bmatrix} F_1\\ F_2\\ F_3\\ M_1\\ M_2\\ M_3 \end{bmatrix} = \begin{bmatrix} S_{11} & S_{12} & S_{13} & S_{14} & S_{15} & S_{16}\\ S_{12} & S_{22} & S_{23} & S_{24} & S_{25} & S_{26}\\ S_{13} & S_{23} & S_{33} & S_{34} & S_{35} & S_{36}\\ S_{14} & S_{24} & S_{34} & S_{44} & S_{45} & S_{46}\\ S_{15} & S_{25} & S_{35} & S_{45} & S_{55} & S_{56}\\ S_{16} & S_{26} & S_{36} & S_{46} & S_{56} & S_{66} \end{bmatrix} \begin{bmatrix} \gamma_{11}\\ 2\gamma_{12}\\ 2\gamma_{13}\\ \kappa_1\\ \kappa_2\\ \kappa_3 \end{bmatrix} \quad \text{or} \quad \begin{bmatrix} \boldsymbol{F}\\ \boldsymbol{M} \end{bmatrix} = [\boldsymbol{S}] \begin{bmatrix} \boldsymbol{\gamma}\\ \boldsymbol{\kappa} \end{bmatrix}
\tag{3}
$$

where $\boldsymbol{S}$ contains the stiffness components of the composite blade cross section. All the cross-sectional quantities mentioned previously are calculated by using the cross-sectional analysis software VABS (version 3.7.1), which has been extensively validated and used in composite beam applications [34]. It is noted that, in this study, the extensional–torsional coupling S_{14} and bend–twist coupling S_{46} of the composite lamination is of great interest. By premultiplying Eq. (3) by $[\boldsymbol{S}]^{-1}$ and substituting into the equations of motion [Eq. (1)], the dependency of the equations to the generalized strains can be removed.

To close the composite blade equations, it is necessary to define the boundary conditions of the blade. The blade is a hingeless rotor blade that is completely fixed at the rotor hub and free at the tip. Therefore, the following set of boundary conditions is applied to the equations of motion:

$$
\begin{bmatrix} F_1(L,t)\\ F_2(L,t)\\ F_3(L,t) \end{bmatrix} = \begin{bmatrix} 0\\ 0\\ 0 \end{bmatrix}, \quad \begin{bmatrix} M_1(L,t)\\ M_2(L,t)\\ M_3(L,t) \end{bmatrix} = \begin{bmatrix} 0\\ 0\\ 0 \end{bmatrix},
$$

$$
\begin{bmatrix} V_1(0,t)\\ V_2(0,t)\\ V_3(0,t) \end{bmatrix} = \begin{bmatrix} 0\\ 0\\ 0 \end{bmatrix}, \quad \begin{bmatrix} \Omega_1(0,t)\\ \Omega_2(0,t)\\ \Omega_3(0,t) \end{bmatrix} = \begin{bmatrix} 0\\ 0\\ \Omega_0 \end{bmatrix}
\tag{4}
$$

To solve the governing equations of the blade, a space–time discretization scheme with second-order accuracy has been used [30]. In this method, any variable in the equations of motion are defined on the left and right sides of each node. This is appropriate to take into account any discontinuity such as the concentrated mass. The details of the solution method can be found in Ref. [30]. It is noted that, in this study, by considering 16 elements distributed uniformly, convergent results are obtained.

Finally, the equations of motion are summarized in a compact form as

$$a_{ji}\dot{\boldsymbol{q}}_i + b_{ji}\boldsymbol{q}_i + c_{jik}\boldsymbol{q}_i\boldsymbol{q}_k = 0 \tag{5}$$

where q is the vector containing the unknown parameters (F_i, M_i, V_i, Ω_i, $i = 1, \ldots, 3$) at the left and right sides of each node; and a, b, and c are the matrices of linear and nonlinear coefficients. First, the steady-state condition of the system is determined by removing all time derivative terms and solving the resultant nonlinear equations by the Newton–Raphson method. If required, the equations of motion may be linearized about this steady-state condition in order to obtain the rotating frequencies of the blade through eigenvalue analysis.

IV. Verification of the Code

To check the developed analytical model for the composite blade, several numerical examples are completed and compared with those reported in the literature. First, to evaluate the dynamic behavior of the developed composite blade model without a concentrated mass, the rotating natural frequencies of a composite blade with the material properties presented in Table 1 are determined and compared with the detailed finite element results [35]. Here, the blade cross section is a rectangular composite box composed of six plies, with a thickness of 0.127 mm for each ply. The outer beam box has a width of 24.2 mm and a height of 13.5 mm, and it has a blade length of 845 mm, with a mass density of 1445 kg/m^3. The sign convention for the layup angle is shown in Fig. 2, where θ is the ply fiber orientation. Table 2 shows that the correlation between the results is very good, which means that the dynamics of the developed composite blade model works well.

To check the convergence of the method of the solution, the variation of the first flap frequency of the aforementioned case with respect to the number of elements along the span of the blade is determined and shown in Fig. 3. By using about 16 elements, the results have converged sufficiently; therefore, the number of elements used to solve the 1-D beam equations in the examples is 16.

The effect of adding a concentrated mass on the frequency parameter of an isotropic beam has been determined and compared with the results obtained by Wright et al. [36], and it is reported in

Table 1 Material properties of the composite box-beam (AS4-3501-6)

Parameter	Value
E_1, GPa	142
E_2, GPa	9.8
G_{12}, GPa	6.13
ν_{12}	0.42
ρ, kg/m^3	1445

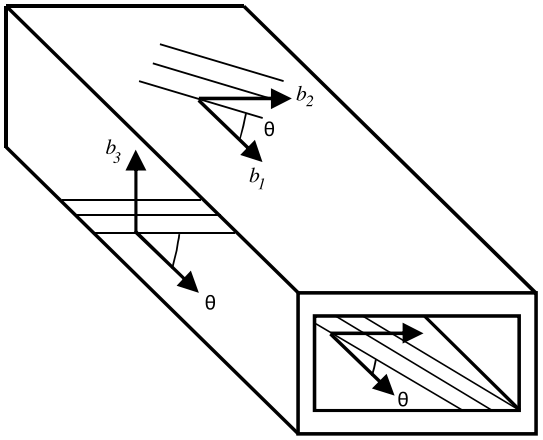

Fig. 2 Composite box beam sign convention.

Fig. 4. In this case, the concentrated mass is located at the tip of the blade and the mass ratio is $\beta = m_p/m_L = 1$. It is clear that the obtained frequency parameters ($\omega_n = q_n.\sqrt{mR^4/EI}$) are a good match.

V. Effect of the Moving Mass on the Blade Twist

In what follows, the effect of adding a concentrated mass to the composite blade and its effect on the twist are examined. The composite blade used here is the same as the one used by Smith and Chopra [35], which is representative of a scaled blade for experiments. Three layups for the composite box are considered here and are shown in Table 3. The first case (case 1) layup is antisymmetric and represents extension–torsion coupling, whereas the second case (case 2) is a symmetric case considered for bending–torsion coupling. Finally, the third case is a general representation of the second symmetric case. The first two cases are considered because the first one is applicable for twist change when the concentrated mass moves in the spanwise direction, and the second case works well when the concentrated mass moves in the chordwise direction.

The corresponding stiffness matrices generated by VABS for case 1 and case 2 of the composite cross section are presented as follows:

$$[S]_{\text{case1}} = \begin{bmatrix} 5.69\times10^{6} & 0 & 0 & -7.89\times10^{3} & 0 & 0 \\ 0 & 4.10\times10^{5} & 0 & 0 & 5.27\times10^{3} & 0 \\ 0 & 0 & 2.03\times10^{5} & 0 & 0 & 2\times10^{3} \\ -7.89\times10^{3} & 0 & 0 & 5.02\times10^{1} & 0 & 0 \\ 0 & 5.27\times10^{3} & 0 & 0 & 1.87\times10^{2} & 0 \\ 0 & 0 & 2.00\times10^{3} & 0 & 0 & 4.29\times10^{2} \end{bmatrix}$$

$$[S]_{\text{case2}} = \begin{bmatrix} 5.09\times10^{6} & 6.57\times10^{2} & 3.05\times10^{5} & 1.12\times10^{2} & 5.35\times10^{3} & -2.76\times10^{2} \\ 6.57\times10^{2} & 4.19\times10^{5} & 2.40\times10^{2} & -3.39\times10^{1} & -4.81\times10^{1} & 7.79\times10^{1} \\ 3.05\times10^{5} & 2.40\times10^{2} & 1.76\times10^{5} & 3.82\times10^{0} & 2.87\times10^{2} & -2.76\times10^{1} \\ 1.12\times10^{2} & -3.39\times10^{1} & 3.82\times10^{0} & 5.04\times10^{1} & 0 & -4.26\times10^{1} \\ 5.35\times10^{3} & -4.81\times10^{1} & 2.87\times10^{2} & 0 & 1.53\times10^{2} & 0 \\ -2.76\times10^{2} & 7.79\times10^{1} & -2.76\times10^{1} & -4.33\times10^{1} & 0 & 3.55\times10^{2} \end{bmatrix}$$

Moreover, the mass per unit length and the mass moment of inertia of the composite beam are presented in Table 4.

It is noted that, in this study, about 1320 quadrilateral elements with 8 nodes are used to discretize the cross section of the blade. The mesh refinement study of the cross section for the bend–twist coupling value with respect to different numbers of elements is shown in Fig. 5, and it shows that 1320 elements are sufficient.

Table 2 Comparison of the rotating natural frequencies (in hertz) for the symmetric layup ($[15]_3$, $[15/-15]_3$) at $\Omega = 1002$ rpm

Mode	Present	Detailed finite element method [35]
Flap 1	35.407	36
Flap 2	195.518	197.3
Lag 1	56.722	57.1
Lag 2	351.099	349.3
Torsion 1	713.706	714.9

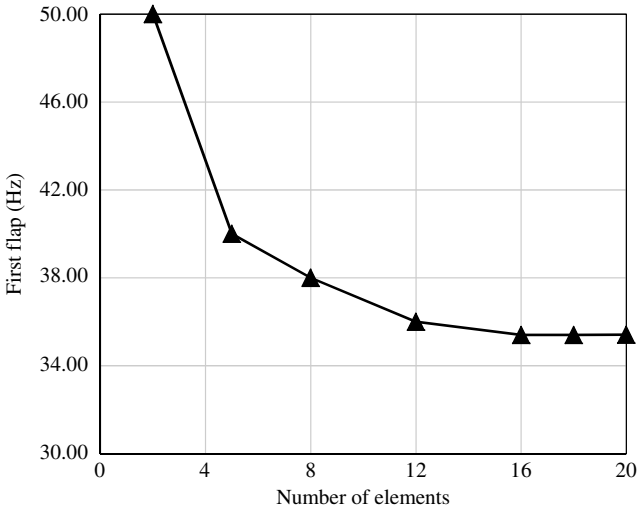

Fig. 3 Convergence of the method of solution for the first rotating frequency.

First, the twist distribution along the span of the blade and its variation with the movement of the mass are examined. Figure 6 shows the twist distribution of the case 1 blade for two spanwise positions of the concentrated mass. It is clear that, by moving the mass from the root to the tip of the blade, the twist distribution changes and the trend of the twist remains the same. It is noted that, in this case, even when there is no additional mass ($x_p/l = 0$), the twist distribution of the blade changes. This twist change is due to the blade mass itself and the composite tailoring because the blade was initially straight without any pretwist.

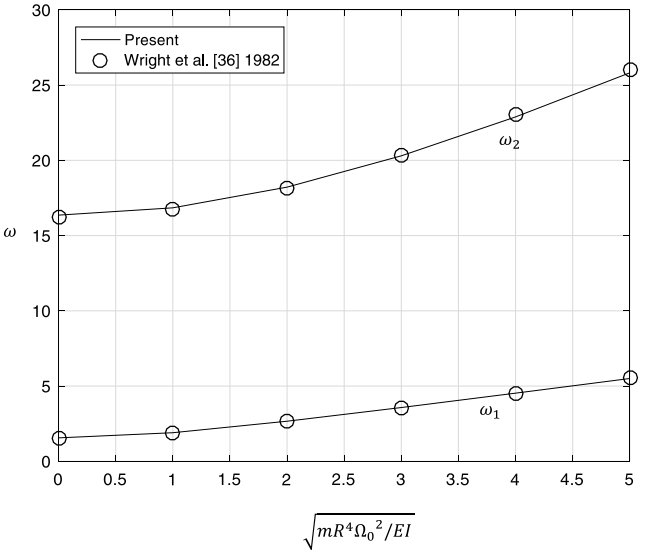

Fig. 4 Comparison of the change in frequency parameter with respect to the nondimensional rotating speed for an isotropic beam with a concentrated mass.

Table 3 Composite blade layup configurations

Configuration	Top wall	Bottom wall	Right wall	Left wall
Case 1	$[15]_6$	$[-15]_6$	$[15/-15]_3$	$[-15/15]_3$
Case 2	$[15/-15]_3$	$[15/-15]_3$	$[15]_6$	$[15]_6$
General case 2	$[\theta/-\theta]_3$	$[\theta/-\theta]_3$	$[\theta]_6$	$[\theta]_6$

Table 4 Mass properties of the composite blade

Parameter	Value
m, kg/m	7.92×10^{-2}
i_2, kg · m	2.46×10^{-6}
i_3, kg · m	6.22×10^{-6}

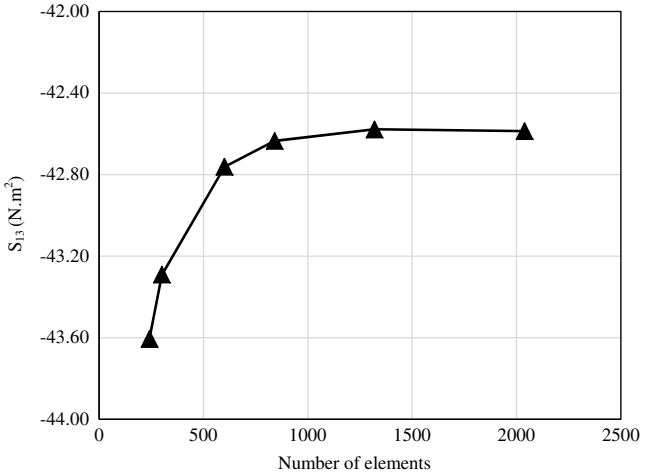

Fig. 5 Mesh convergence to calculate the bend–twist coupling value.

Figure 7 also demonstrates the spanwise twist distribution of the blade for two different chordwise locations of the concentrated mass. When the mass moves from the trailing edge to the leading edge, not only the twist distribution of the blade changes but also the trend of the twist changes. Therefore, the spanwise and chordwise locations

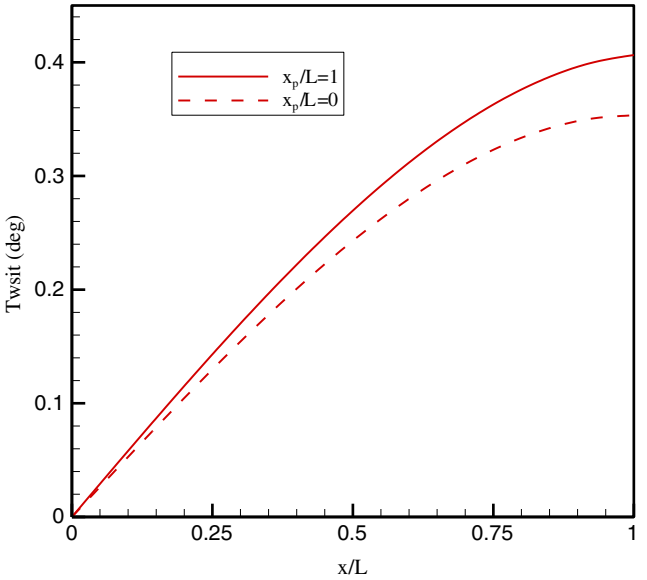

Fig. 6 Twist distribution of the composite blade case 1 ($\beta = 0.05$, $y_p = 0$, and $\Omega_0 = 1000$ rpm).

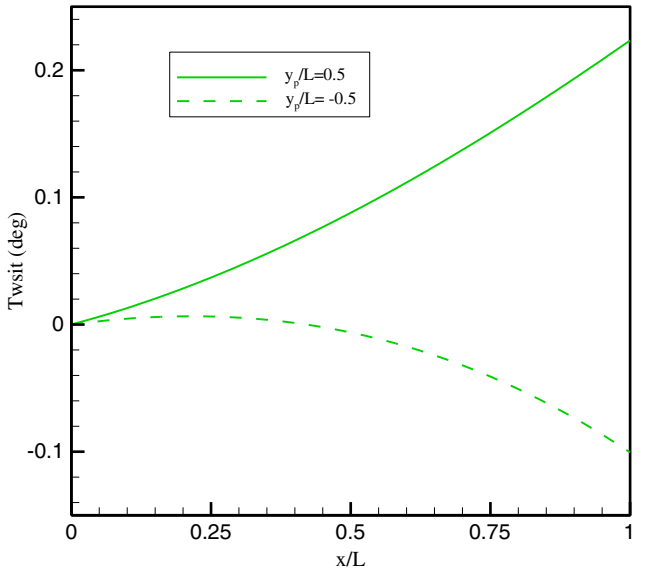

Fig. 7 Twist distribution of the composite blade case 2 ($\beta = 0.05$, $x_p = 1$, and $\Omega_0 = 1000$ rpm).

of the concentrated mass have significant effects on this morphing concept.

Figures 8 and 9 show the effects of the spanwise x_p and chordwise y_p movements of the concentrated mass for the two layup cases. Figure 6 shows that, when the extension–torsion coupling is present, the spanwise location of the concentrated mass is important; whereas for the bending–torsion coupling case (Fig. 7), the chordwise position of the concentrated mass affects the twist variation of the blade. The overall chord of the blade is $c = 66$ mm.

The chordwise location of the concentrated mass with different mass ratios for the symmetric case is shown in Fig. 10. When the mass ratio is $\beta = 0.05$ and the mass moves from the leading edge to the trailing edge of the airfoil, about $\delta q = 0.3$ deg of tip twist variation is obtained (here, the twist angle is denoted by q).

Next, the effect of different fiber orientations of the ply angle θ for the symmetric case (general case 2) on the tip twist angle variation is considered for different mass ratios, and Fig. 11 shows the results. It is assumed that the concentrated mass moves from the leading edge to

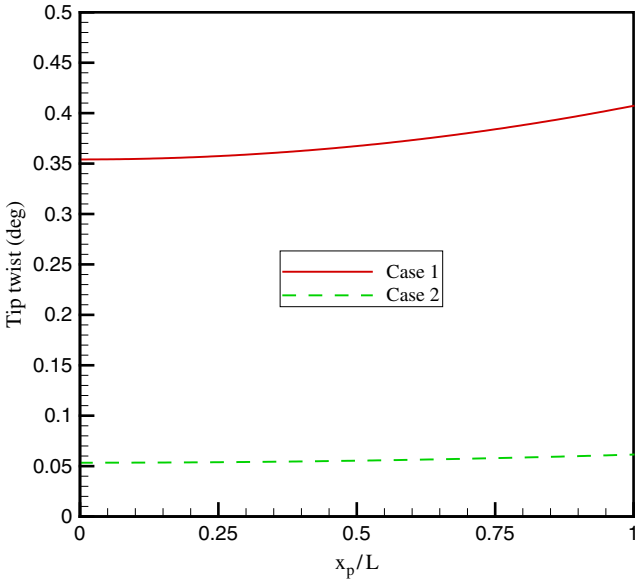

Fig. 8 The effect of the concentrated mass spanwise location on the tip twist variation for different composite cases ($\beta = 0.05$, $y_p = 0$, and $\Omega_0 = 1000$ rpm).

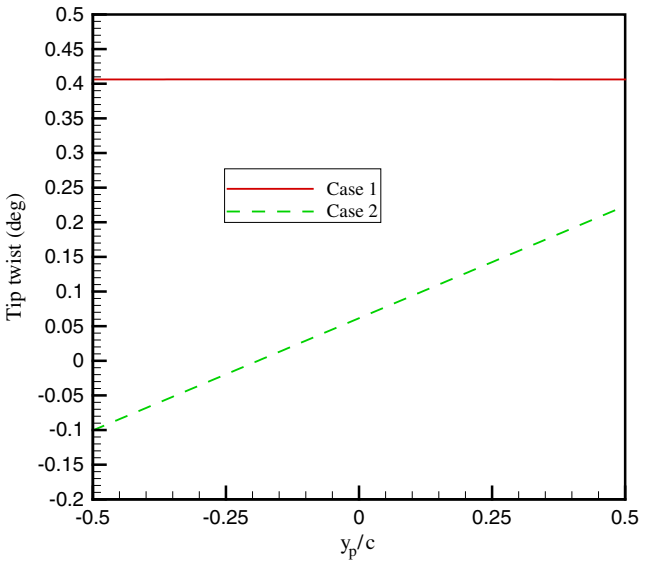

Fig. 9 Tip twist distribution with respect to the chordwise location for different composite cases ($\beta = 0.05$, $x_p/L = 1$, and $\Omega_0 = 1000$ rpm).

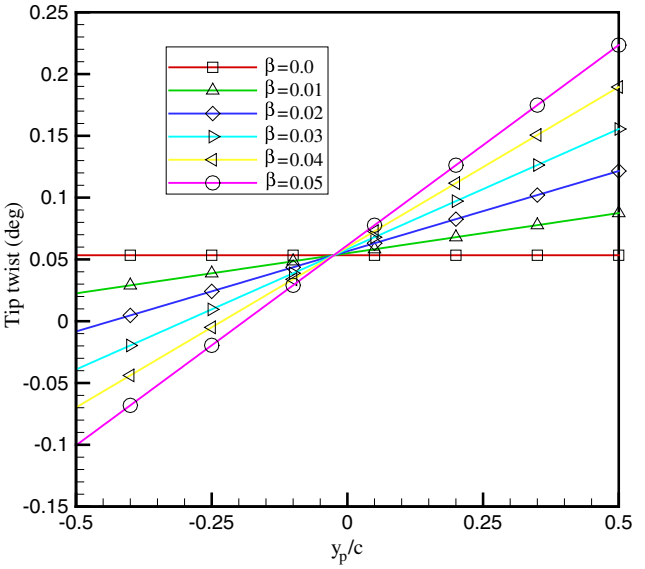

Fig. 10 Tip twist distribution with respect to the chordwise location for different mass ratios (case 2, $x_p/L = 1$, and $\Omega_0 = 1000$ rpm).

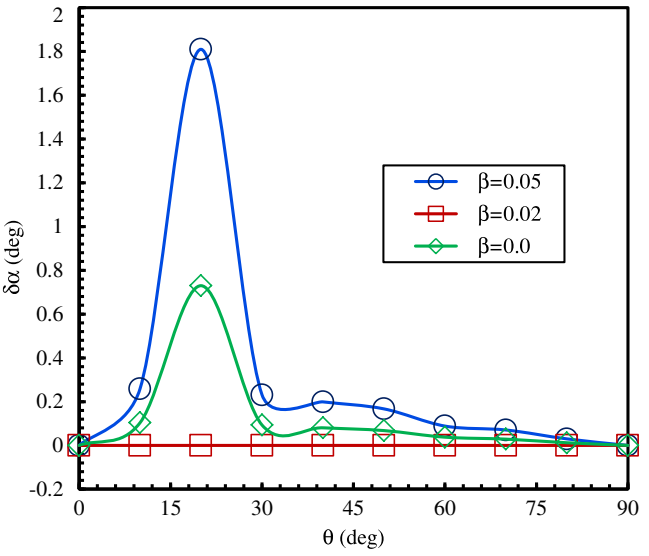

Fig. 11 Tip twist variation with respect to the ply angle for different mass ratios (case 2, $x_p/L = 1$, and $\Omega_0 = 1000$ rpm).

the trailing edge of the cross section, and the tip twist variation is the difference between the blade tip twist of these two locations. When the ply angle is considered to be $\theta = 20$ deg, about a $\delta q = 1.8$ deg tip twist variation is feasible. To examine why this ply angle gives the highest tip twist change, the variation of the nondimensional bend–twist coupling [37–39] index, defined here as $\alpha = S_{46}/\sqrt{S_{44}.S_{66}}$, is determined and plotted in Fig. 10. It is noted that this bend–twist coupling term can be a number within the range $-1 \leq \alpha \leq 1$ [40].

By checking Fig. 12, it is obvious that the highest bend–twist coupling index for this case occurs when the ply angle is equal to $\theta = 20$ deg, and therefore, the maximum tip twist is obtained for this ply angle. The bend–twist coupling depends on the material type, the ply angle of the lamination, and the section geometry; other literature reported that the highest value of this coupling occurred for ply angles between 15 and 30 deg [40], and so this value is typical.

It is noted that, as the blade considered here is a scaled blade (and the length of the blade is small in comparison to a real blade), the effect of this concept on a real scale blade is also required to be investigated. Therefore, a blade resembling the main rotor blade of the BO-105 is considered next [41]. It is assumed that the blade has uniform spanwise properties, unlike the BO-105 blade; and it has fundamental flap, lag, and torsional frequencies similar to the BO-105 main rotor blade. The blade characteristics are presented in Table 5.

To compare to this blade, it was first necessary to define a tailored blade that was equivalent to the BO-105 blade. A generic algorithm optimization was used to select the torsional, lagwise bending, and flapwise bending stiffnesses, as well as the sectional inertial of the blade, to give similar modal frequencies to the original blade. Table 6 shows the comparison between the fundamental rotating frequencies of the blade considered here by the optimization method, as well as those reported in Ref. [41].

By moving an added mass with different mass ratios located at the tip of the blade along the chord of the blade, the tip twist change of the blade is determined for different values of the bend–twist coupling index α and depicted in Fig. 13. As is clear from this plot, a considerable value of twist change can be induced in the blade.

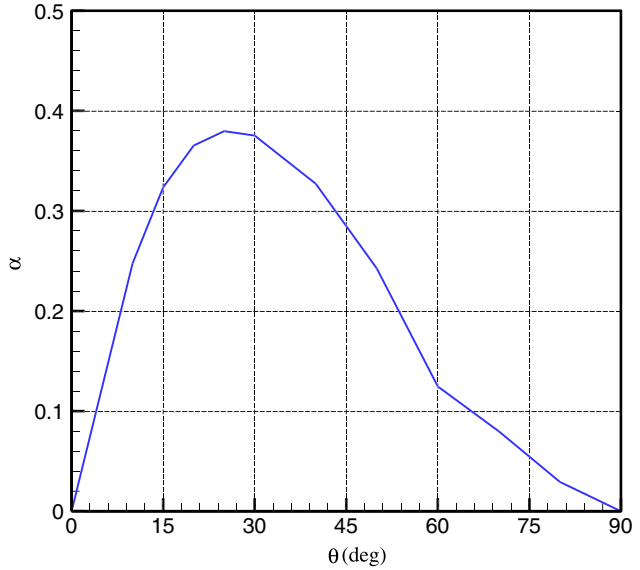

Fig. 12 Bend–twist coupling index for various ply angles (general case 2).

Table 5 BO-105 main rotor blade characteristics [41]

Item	Value
Radius, m	4.91
Chord, m	0.27
Linear pretwist, deg	−8 deg
Precone angle, deg	2.5 deg
Rotating velocity, rad/s	44.4

Table 6 Comparison of the fundamental frequencies of the BO-105 main rotor blade and the present blade

Mode	Present, Hz	Peterson et al. [41], Hz
First lag	4.58	4.66
First flap	7.89	7.91
First torsion	25.31	26.78

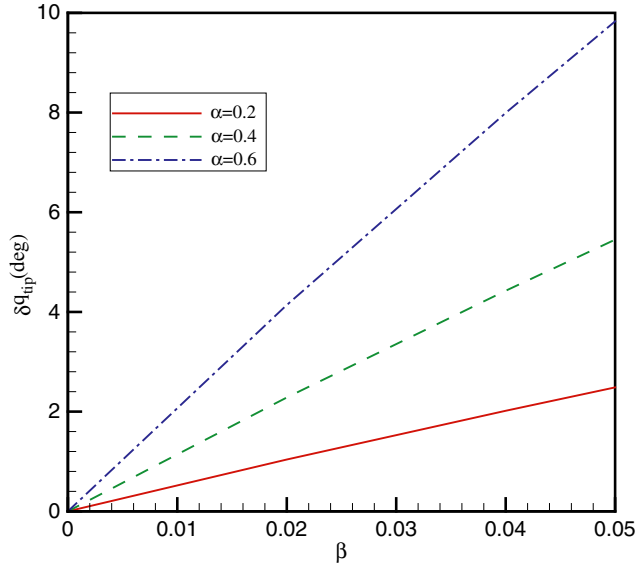

Fig. 13 Tip twist change of the BO-105 blade with respect to various values of mass ratios and the bend–twist coupling index.

When the coupling index is $\alpha = 0.6$ and the added mass is $\beta = 0.05$, about a $\delta q = 10$ deg tip twist change is introduced in the system by moving the mass from the leading edge to the trailing edge of the blade. Therefore, this morphing concept has the potential to be used as a means of twist change in a real blade.

VI. Conclusions

A new concept for changing the twist of a composite blade was introduced and examined. The actuation mechanism for changing the twist of the blade was a concentrated mass that could be moved in the spanwise or chordwise direction of the blade. By moving the mass, a variable centrifugal force or bending moment could be produced that could change the twist of the blade through the extension–twist coupling or the bend–twist coupling of the composite layup. The blade was modeled by using the geometrically exact fully intrinsic beam equations. A composite scaled blade was considered first to analyze the sensitivity of different parameters on the concept, and then a blade with properties similar to the BO-105 main rotor blade was introduced to show the effectiveness of the concept on a real blade. The obtained results were in good agreement with those reported in the literature. The following conclusions are based on the analysis carried out in this paper:

1) In the antisymmetric layup, the spanwise position of the concentrated mass has a major effect on the twist variation and, by locating it at the tip of the blade, the maximum twist can be achieved.

2) When the lamination of the composite box is symmetric, the chordwise location of the mass affects the twist distribution of the blade dramatically. Maximum twist is obtained when the concentrated mass is at the leading or trailing edges of the chord.

3) In the symmetric lamination, when the ply angle is equal to $\theta = 20$ deg, the maximum tip twist variation of about $\delta q = 1.8$ deg occurs. This ply angle is representative of the highest bending–torsion coupling in this case.

5) By moving a mass equal to the 5% mass of the BO-105 blade along the chord, a considerable amount of twist change is induced in the blade.

Overall, this work has given a strong positive indication of the feasibility of the TWIST concept for helicopter blade morphing. However, because adding a mass and introducing stiffness tailoring to the blade could change the stability characteristics, the aeroelastic stability of the system subjected to the added mass needed to be investigated. This and many other issues needed to further develop the TWIST concept are the subject of ongoing work by the authors.

Acknowledgment

The work presented in this paper was funded by the European Union Horizon 2020 Program through the project “Shape Adaptive Blades for Rotorcraft Efficiency (SABRE)” under grant agreement 723491.

References

[1] Johnson, W., *Helicopter Theory*, Princeton Univ. Press, Princeton, NJ, 1980, pp. 11–20.

[2] Barbarino, S., Bilgen, O., Ajaj, R. M., Friswell, M. I., and Inman, D. J., “A Review of Morphing Aircraft,” *Journal of Intelligent Material Systems and Structures*, Vol. 22, No. 9, 2011, pp. 823–877. doi:10.1177/1045389X11414084

[3] Maucher, C. K., Grohmann, B. A., and Jäker, P., “Review of Adaptive Helicopter Rotor Blade Actuation Concepts,” *Proceedings of the 9th Adaptronic Congress*, Göttingen, Germany, 2005.

[4] Straub, F. K., “A Feasibility Study of Using Smart Materials for Rotor Control,” *Smart Materials and Structures*, Vol. 5, No. 1, 1996, Paper 1. doi:10.1088/0964-1726/5/1/002

[5] Chopra, I., “Review of State of Art of Smart Structures and Integrated Systems,” *AIAA Journal*, Vol. 40, No. 11, 2002, pp. 2145–2187. doi:10.2514/2.1561

[6] Mistry, M., Gandhi, F., Nagelsmit, M., and Gurdal, Z., “Actuation Requirements of a Warp-Induced Variable Twist Rotor Blade,” *Journal of Intelligent Material Systems and Structures*, Vol. 22, No. 9, 2011, pp. 919–933. doi:10.1177/1045389X11404957

[7] Han, D., Pastrikakis, V., and Barakos, G. N., “Helicopter Flight Performance Improvement by Dynamic Blade Twist,” *Aerospace*

Science and Technology, Vol. 58, Sept. 2016, pp. 445–452. doi:10.1016/j.ast.2016.09.013

[8] Chen, P. C., and Chopra, I., "Induced Strain Actuation of Composite Beams and Rotor Blades with Embedded Piezoceramic Elements," *Smart Materials and Structures*, Vol. 5, No. 1, 1996, Paper 35. doi:10.1088/0964-1726/5/1/005

[9] Chen, P. C., and Chopra, I., "Hover Testing of Smart Rotor with Induced-Strain Actuation of Blade Twist," *AIAA Journal*, Vol. 35, No. 1, 1997, pp. 6–16. doi:10.2514/2.74

[10] Chattopadhyay, A., Liu, Q., and Gu, H., "Vibration Reduction in Rotor Blades Using Active Composite Box Beam," *AIAA Journal*, Vol. 38, No. 7, 2000, pp. 1125–1131. doi:10.2514/2.1097

[11] Cesnik, C. E. S., Shin, S., and Wilbur, M. L., "Dynamic Response of Active Twist Rotor Blades," *Smart Materials and Structures*, Vol. 10, No. 1, 2001, Paper 62. doi:10.1088/0964-1726/10/1/306

[12] Shin, S.-J., and Cesnik, C., "Forward Flight Response of the Active Twist Rotor for Helicopter Vibration Reduction," *19th AIAA Applied Aerodynamics Conference*, AIAA Paper 2001-1357, 2001.

[13] Thakkar, D., and Ganguli, R., "Helicopter Vibration Reduction in Forward Flight with Induced-Shear Based Piezoceramic Actuation," *Smart Materials and Structures*, Vol. 13, No. 3, 2004, Paper 599. doi:10.1088/0964-1726/13/3/019

[14] Schultz, M. R., "A Concept for Airfoil-Like Active Bistable Twisting Structures," *Journal of Intelligent Material Systems and Structures*, Vol. 19, No. 2, 2008, pp. 157–169. doi:10.1177/1045389X06073988

[15] Pawar, P. M., and Jung, S. N., "Active Twist Control Methodology for Vibration Reduction of a Helicopter with Dissimilar Rotor System," *Smart Materials and Structures*, Vol. 18, No. 3, 2009, Paper 035013. doi:10.1088/0964-1726/18/3/035013

[16] You, Y. H., Jung, S. N., and Kim, C. J., "Optimal Deployment Schedule of an Active Twist Rotor for Performance Enhancement and Vibration Reduction in High-Speed Flights," *Chinese Journal of Aeronautics*, Vol. 30, No. 4, 2017, pp. 1427–1440. doi:10.1016/j.cja.2017.04.017

[17] Prahlad, H., and Chopra, I., "Design of a Variable Twist Tilt-Rotor Blade Using Shape Memory Alloy (SMA) Actuators," *SPIE's 8th Annual International Symposium on Smart Structures and Materials*, Vol. 42327, Soc. of Photo-Optical Instrumentation Engineers, Bellingham, WA, 2001, pp. 46–59. doi:10.1117/12.436559

[18] Bushnell, G. S., Arbogast, D., and Ruggeri, R., "Shape Control of a Morphing Structure (Rotor Blade) Using a Shape Memory Alloy Actuator System," *Proceedings of the SPIE Smart Structures and Materials*, Vol. 6928, Soc. of Photo-Optical Instrumentation Engineers, 2008, Paper 69282A. doi:10.1117/12.775927

[19] Ruggeri, R. T., Jacot, A. D., and Clingman, D. J., "Shape Memory Actuator Systems and the Use of Thermoelectric Modules," *SPIE's 9th Annual International Symposium on Smart Structures and Materials*, Vol. 4698, SPIE, Bellingham, WA, 2002, Paper 9.

[20] Ruggeri, R., Arbogast, D., and Bussom, R., "Wind Tunnel Testing of a Lightweight One-Quarter-Scale Actuator Utilizing Shape Memory Alloy," *49th AIAA/ASME/ASCE/AHS/ASC Structures, Structural Dynamics, and Materials Conference, 16th AIAA/ASME/AHS Adaptive Structures Conference,10th AIAA Non-Deterministic Approaches Conference, 9th AIAA Gossamer Spacecraft Forum, 4th AIAA Multidisciplinary Design Optimization Specialists Conference*, AIAA Paper 2008-2279, 2008.

[21] Clingman, D., and Jacot, D., "Shape Memory Alloy Consortium and Demonstration," *41st Structures, Structural Dynamics, and Materials Conference and Exhibit*, AIAA Paper 2000-1790, 2000.

[22] Vos, R., Gurdal, Z., and Abdalla, M., "Mechanism for Warp-Controlled Twist of a Morphing Wing," *Journal of Aircraft*, Vol. 47, No. 2, 2010, pp. 450–457. doi:10.2514/1.39328

[23] Nixon, M. W., "Aeroelastic Response and Stability of Tiltrotors with Aeroelastically-Coupled Composite Rotor Blades," Ph.D. Dissertation, Univ. of Maryland, College Park, MD, 1993.

[24] Soykasap, O., and Hodges, D. H., "Performance Enhancement of a Composite Tilt-Rotor Using Aeroelastic Tailoring," *Journal of Aircraft*, Vol. 37, No. 5, 2000, pp. 850–858. doi:10.2514/2.2680

[25] Byers, L., "Helicopter Rotor Lag Damping Augmentation Based on Radial Absorber and Coriolis Coupling," Ph.D. Dissertation, Pennsylvania State Univ., State College, PA, 2006.

[26] Byers, L., and Gandhi, F., "Embedded Absorbers for Helicopter Rotor Lag Damping," *Journal of Sound and Vibration*, Vol. 325, No. 4, 2009, pp. 705–721. doi:10.1016/j.jsv.2009.03.031

[27] Austruy, J., Gandhi, F., and Lieven, N., "Rotor Vibration Reduction Using an Embedded Spanwise Absorber," *Journal of the American Helicopter Society*, Vol. 57, No. 2, 2012, pp. 49–60.

[28] Kang, H., "Blade Lag Damping Using Embedded Chordwise Absorbers," Ph.D. Dissertation, Pennsylvania State Univ., State College, PA, 2001.

[29] Petrie, J., "Helicopter Rotor Blade Lag Damping Using Fluid Elastic Embedded Chordwise Inertial Dampers," M.S. Dissertation, Pennsylvania State Univ., State College, PA, 2004.

[30] Hodges, D. H., "Geometrically Exact, Intrinsic Theory for Dynamics of Curved and Twisted Anisotropic Beams," *AIAA Journal*, Vol. 41, No. 6, 2003, pp. 1131–1137. doi:10.2514/2.2054

[31] Amoozgar, M. R., Shahverdi, H., and Nobari, A. S., "Aeroelastic Stability of Hingeless Rotor Blades in Hover Using Fully Intrinsic Equations," *AIAA Journal*, Vol. 55, No. 7, 2017, pp. 2450–2460. doi:10.2514/1.J055079

[32] Sotoudeh, Z., and Hodges, D. H., "Structural Dynamics Analysis of Rotating Blades Using Fully Intrinsic Equations, Part I: Formulation and Verification of Single-Load-Path Configurations," *Journal of the American Helicopter Society*, Vol. 58, No. 3, 2013, pp. 1–9.

[33] Amoozgar, M. R., and Shahverdi, H., "Analysis of Nonlinear Fully Intrinsic Equations of Geometrically Exact Beams Using Generalized Differential Quadrature Method," *Acta Mechanica*, Vol. 227, No. 5, 2016, pp. 1265–1277. doi:10.1007/s00707-015-1528-7

[34] Yu, W., Hodges, D. H., Volovoi, V., and Cesnik, C. E. S., "On Timoshenko-Like Modeling of Initially Curved and Twisted Composite Beams," *International Journal of Solids and Structures*, Vol. 39, No. 19, 2002, pp. 5101–5121. doi:10.1016/S0020-7683(02)00399-2

[35] Smith, E. C., and Chopra, I., "Aeroelastic Response, Loads, and Stability of a Composite Rotor in Forward Flight," *AIAA Journal*, Vol. 31, No. 7, 1993, pp. 1265–1273. doi:10.2514/3.49066

[36] Wright, A. D., Smith, C. E., Thresher, R. W., and Wang, J. L. C., "Vibration Modes of Centrifugally Stiffened Beams," *Journal of Applied Mechanics*, Vol. 49, No. 1, 1982, pp. 197–202. doi:10.1115/1.3161966

[37] Kobayashi, A., "Achievements in Composites in Japan and United States.," *Fifth Japan–US Conference on Composite Materials*, Tokyo, June 1990, pp. 687–694.

[38] Hodges, D. H., Nixon, M. W., and Rehfield, L. W., "Comparison of Composite Rotor Blade Models: A Coupled-Beam Analysis and an MSC/NASTRAN Finite-Element Model," NASA TM 89024, 1987.

[39] Rehfield, L. W., "Design Analysis Methodology for Composite Rotor Blades," *Proceedings of the 7th DoD/NASA Conference on Fibrous Composites in Strcutural Design*, Paper AFWAL-TR-85-3094, Denver, CO, June 1985, pp. (V(a)-l)–(V(a)-15).

[40] Ong, C. H., Wang, J., and Tsai, S. W., "Design, Manufacturing and Testing of a Bend-Twist D-Spar," *37th Aerospace Sciences Meeting and Exhibit Reno*, AIAA Paper 1999-0025, 1999. doi:10.2514/6.1999-25

[41] Peterson, R. L., Field, M., Johnson, W., and Alto, P., "Aeroelastic Loads and Stability Investigation of a Full-Scale Hingeless Rotor," NASA TM 103867, 1991.

C. Bisagni
Associate Editor